Numerical Simulations of Gust Front / Microburst Collision Dynamics

Leigh Orf

Department of Atmospheric Science
University of North Carolina at Asheville
Asheville, North Carolina USA 28804
orf@unca.edu

1 Introduction

A microburst is a local, intense downdraft which induces an outburst of damaging winds near the ground which extends 4 km or less. Microbursts are of interest to researchers because of the strong, occasionally damaging surface winds they produce, and the hazardous wind patterns they create for aircraft in the landing or takeoff phases of flight. The dynamics and aircraft hazards posed by an isolated microburst are well understood. Previous work investigating the interaction between colliding microbursts revealed complex dynamical regimes for certain collision geometries (Orf et al. 1996). In some configurations, regions of elevated wind shear were found which would be significantly hazardous to jetliners in the takeoff or landing phases of flight. These hazardous winds were found in regions well outside of the regions typically associated with an isolated microburst.

In this study, the interaction between a microburst and a thunderstorm gust front are investigated using a three-dimensional nonhydrostatic subcloud model. The model is dry, and microbursts and gust fronts are initiated using a cooling forcing function. A two-dimensional gust front is allowed to evolve at one end of the model domain and microbursts are initiated at varying times, leading to collisions ahead of, at, and behind the gust front head. Preliminary results indicate that during collision events, a broad region of enhanced downward and divergent winds develops. This region would pose a threat to aircraft encountering such winds. Regions of intense short-lived vertical vorticity also were found during this simulation, suggesting that so-called "gustnado" circulations are possible from such collisions.

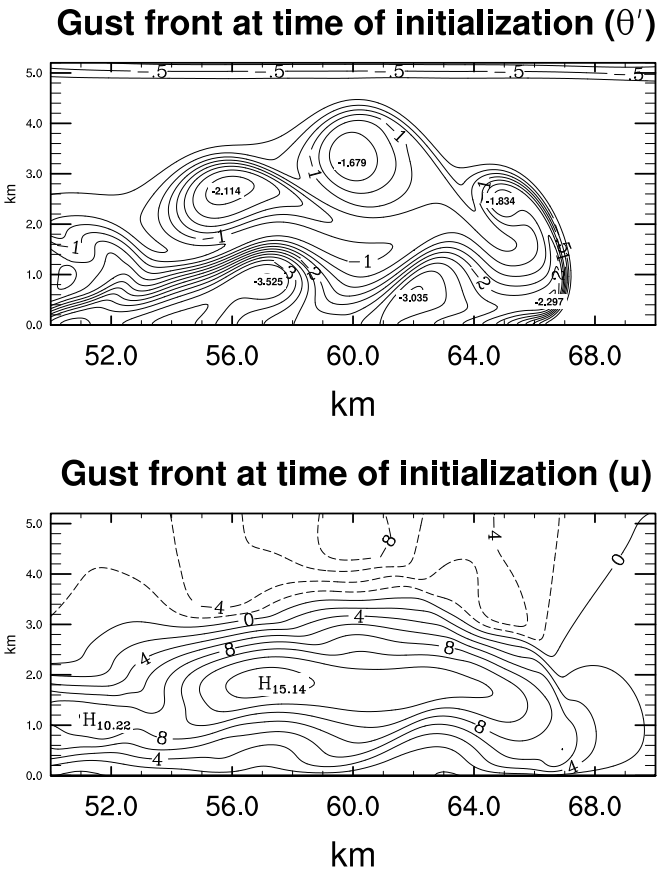

Figure 1: Gust front state at the time of microburst initialization. θ' is contoured every 0.25 K, and u is contoured every 2 m/s.

2 Model initialization

The model used in this study is identical to that described in Orf et al. (1996). The model is a three-dimensional non-hydrostatic quasi-compressible subcloud model without microphysics; all thermal forcings are parametrized. The model is run at 25 meter isotropic resolution in a model domain with dimensions of 900×500×200 gridpoints, or 22.5 km × 12.5 km × 5 km. The sound speed is slowed to 80 m/s, which is greater than twice the fastest physical velocity occurring in the simulations. A constant kinematic eddy viscosity coefficient of 20 m^2/s is used. The model stratification is is dry neutral up to 3 km and slightly stable above, and environmental winds are calm.

The gust front is initialized within a more viscous two-dimensional version of the model and integrated forward for two hours. The kinematic eddy viscosity is doubled to 40 m^2/s in order to provide more mixing, which is artificially small in a two-dimensional model, and to produce a reasonable gust front structure. History files of 2D model prognostics are saved every 30 seconds. Rather than integrating the gust front within the 3D model, a snapshot of the 2D gust front at an appropriate time in its evolution is expanded throughout the 3D model as initial conditions. This is done in order to conserve computational resources. For future integrations, a more realistic 3D gust front structure will be considered; however, because of the difference in spatial scale between a typical microburst and the cold pool of a thunderstorm, the 2D gust front assumption may suffice.

Fig. 1 shows a vertical cross section through the 2D gust front of potential temperature perturbation and horizontal wind speed at the time of microburst initialization. The depth of the gust front head is about 3 km, with maximum horizontal winds behind the gust of 15 m/s at 1.8 km. Observations of thunderstorm outflows show a wide range of gust front depths, and our initial experiment contains a deep gust front. Furthur experiments with outflow collisions will also include shallower thunderstorm outflows.

3 Objectives and Methodology

The main objectives of this study are to explore:

- the spatial and temporal nature of dynamical regimes which would pose a threat to aircraft in the landing and takeoff phase of flight
- the morphology of local regions of intense vorticity created by collision events
- the sensitivity of collision morphology to gust front depth/strength
- the sensitivity of collision morphology to environmental wind shear

Aircraft hazard is gauged by calculating the worst-case 1-km averaged F-factor hazard parameter (Targ and Bowles 1988). The 1-km averaged F-factor is defined as

$$\overline{F} = \frac{1}{g}\overline{\frac{DU}{Dt}} - \frac{\overline{w}}{V_a} \tag{1}$$

where $\overline{\frac{DU}{Dt}}$ is the Lagrangian derivative of the horizontal wind averaged along 1 km of the aircraft path, g is the gravitational acceleration, $\overline{w}$ is the 1 km averaged vertical wind component along the aircraft path, and V_a is the aircraft airspeed, taken to be 75 m/s. The magnitude of the F-factor represents the amount aircraft performance loss due to rapidly changing horizontal winds along the flight path (e.g., a headwind changing to a tailwind), and performance loss due to encounters with descending air, which displaces the aircraft downward. Values of the F-factor exceeding 0.1 over a kilometer's distance are considered hazardous to aircraft below 500 m AGL. Because of the direction-dependent nature of $\overline{F}$, we must calculate $\overline{F}$ for many different flight paths passing through a given gridpoint. At each gridpoint below 500 meters, the aircraft is rotated 360° in 4° increments at a 2° descending glide slope, and the maximum value of $\overline{F}$ occurring over all paths, $\overline{F}_{max}$, is stored to disk, along with the angle which $\overline{F}_{max}$ occurred.

In addition to aircraft hazard, vertical vorticity is calculated in order to explore the nature of misocyclonic circulations which occur in these collisions. Misocyclones have been observed in association with the shear along the edge of a gust front, and have been associated with non-supercell tornadogenesis (Kessinger et al. 1988; Lee and Wilhelmson 1997a; Lee and Wilhelmson 1997b).

Three basic collision geometries are considered: collisions where the microburst outflow is ahead of, at, and behind the thunderstorm gust front. Gust front and microburst initialization is unchanged between simulations, only the spacing between the initializations varies.

4 Collision Events

At this time, three simulations have been integrated, one representing each of the three collision geometries being considered: GFMB1 (microburst outflow is ahead of the gust front), GFMB2 (microburst downdraft impinges gust front head) and GFMB3 (microburst downdraft descends into cold pool behind gust front head).

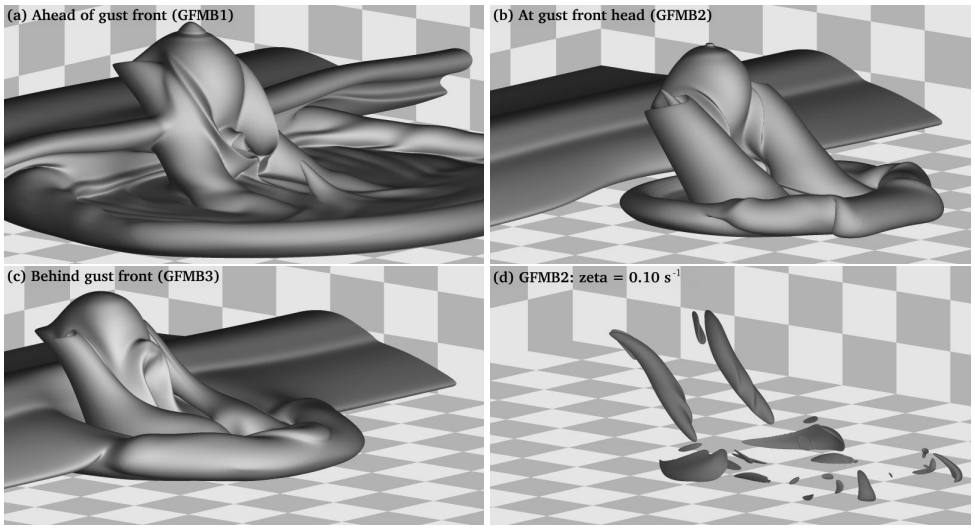

Figure 2: (a) -2K isosurface of θ' for GFMB1 at 1020 seconds (b) -2K isosurface of θ' for GFMB2 at 500 seconds (c) -2K isosurface of θ' for GFMB3 at 500 seconds (d) 0.1 s^{-1} isosurface of $|\zeta|$ for GFMB2 at 600 seconds

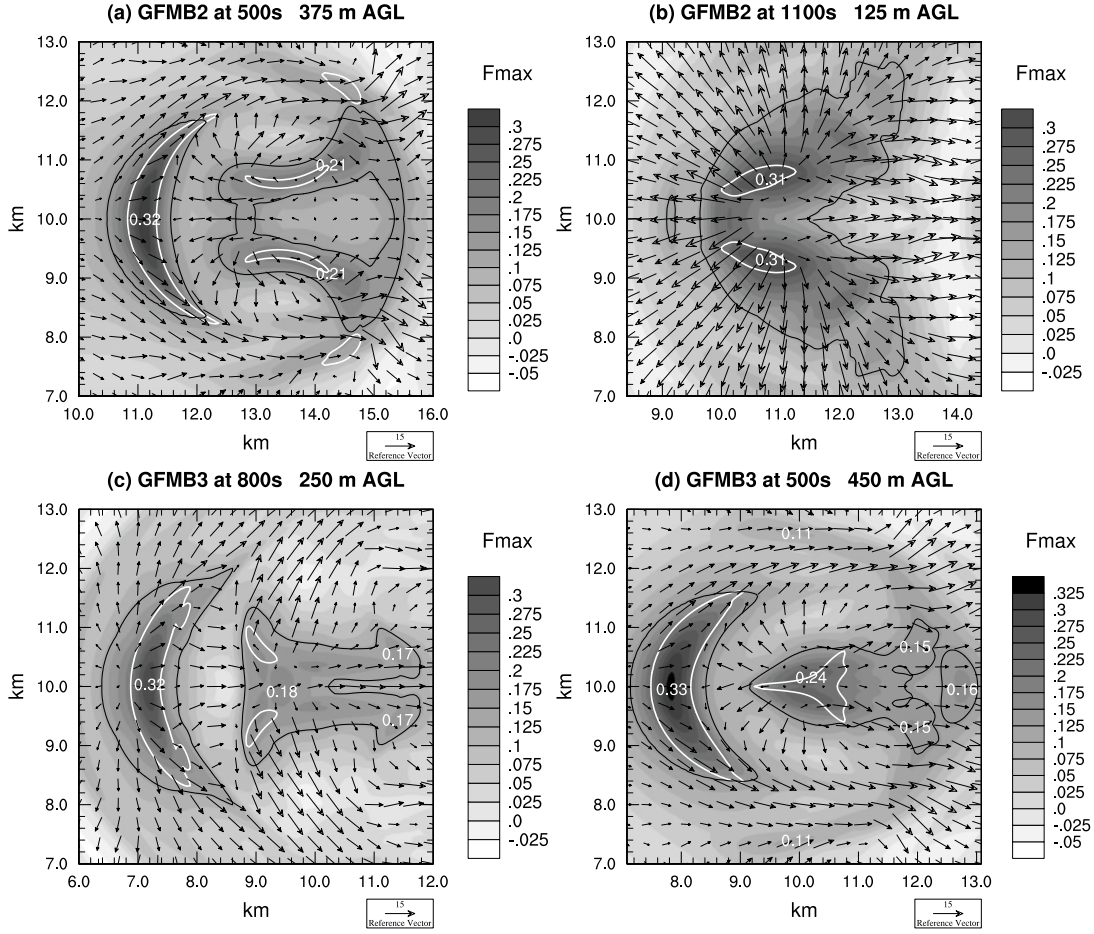

Figure 3: (a) $\overline{F}_{max}$ at 500 s, 375 m AGL for GFMB2. (b) $\overline{F}_{max}$ at 1100 s, 125 m AGL for GFMB2 (c) $\overline{F}_{max}$ at 600 s, 250 m AGL for GFMB3. (d) $\overline{F}_{max}$ at 500 s, 450 m AGL for GFMB3. Black contours represent $\overline{F}_{max} = 0.13$, and white contours represent $w = -10$ m/s. Horizontal wind vectors are plotted every seventh gridpoint. Numbers represent local $\overline{F}_{max}$ maxima.

Figure 2(a)-(c) shows the -2 K θ' isosurface during an instance in all three simulations. The deformation of the microburst downdraft by the gust front is apparent in the asymmetry of the outflow, cleft and lobe instabilities in the microburst outflow, and the barrel-like structure seen flanking the microburst downdraft in all three cases. The latter feature, which indicates rotation along a quasi-vertical axis, is due to the microburst downdraft interacting with the wind shear throughout the thunderstorm outflow, and is responsible for the creation of intense vertical vorticity. The cleft and lobe instabilities in the microburst outflow become much more pronounced later in the simulation.

The magnitude of the vertical component of vorticity, $|\zeta|$, is shown in Fig. 2(d). The two vortex tubes flanking the microburst downdraft persist throughout the GFMB2 and GFMB3 simulations. Values of $|\zeta|$ exceeding 0.20 persist throughout these regions, which are most intense at about 2 km AGL. These circulations are small, with a diameter of about 150 meters, and do not persist long after microburst downdraft winds subside.

Aircraft hazard for GFMB2 and GFMB3 is shown in Fig. 3. Regions of $\overline{F}_{max}$ exceeding 0.13 s^{-1}, the must-alert threshold considered by the Federal Aviation Administration, are outlined in black. The -10 m/s vertical component of the wind is also outlined. The crescent-shaped microburst downdraft is the source of the most intense aircraft hazard above 200 m AGL. Aircraft encountering this region of the flow on a northerly or southerly trajectory would experience the greatest loss in performance. Regions of intense horizontal shear are also apparent near the microburst downdraft and surface outflow. A broad region of hazard also exists up to four kilometers away from the microburst downdraft. Both horizontal shear and descending air are apparent in these regions. It is noteworthy that the gust front alone is not a source of aircraft hazard which exceeds the danger threshold, and that in GFMB2 and GFMB3, the magnitude and spatial extent of the hazardous winds exceeds that which would be found in an isolated microburst in a quiescent environment.

5 Concluding Remarks

This paper demonstrates the ability to capture the fine-scale dynamics of microburst / gust front collisions in three dimensions using a numerical model. Preliminary results show that collisions between a microburst and a gust front can produce deep, broad regions of aircraft hazard which extend beyond what would be expected for an isolated microburst. The generation of intense misocyclonic vortices is also observed. Future work will include increasing the parameter space of collision events, varying the nature of the gust front, including environmental shear in the simulations, and performing a vorticity balance analysis to determine the source of misocyclonic circulations.

6 Acknowledgments

This research was supported by the The University of North Carolina in Asheville and through NSF Grant ATM-9986672. All numerical simulations were carried out on the IBM SP system at the North Carolina Supercomputing Center in Raleigh, NC. Line drawings were created with NCAR Graphics, and isosurface renderings were created with the Persistence of Vision Raytracer (PoVRay).

References

Kessinger, C. J., D. B. Parsons, and J. W. Wilson, 1988: Observations of a storm containing misocyclones, downbursts, and horizontal vortex circulations. *Mon. Wea. Rev.* **116**, 1959–1982.

Lee, B. D. and R. B. Wilhelmson, 1997: The numerical simulation of non-supercell tornadogenesis. Part I: Initiation and evolution of pertornadic misocyclone circulations along a dry outflow boundary. *J. Atmos. Sci.* **54**, 32–60.

Lee, B. D. and R. B. Wilhelmson, 1997: The numerical simulation of non-supercell tornadogenesis. Part II: Evolution of a family of tornadoes along a weak outflow boundary. *J. Atmos. Sci.* **54**, 2387–2415.

Orf, L. G., J. R. Anderson, and J. M. Straka, 1996: A three-dimensional numerical analysis of colliding microburst outflow dynamics. *J. Atmos. Sci.* **53**, 2490–2511.

Targ, R. and R. L. Bowles, 1988: Windshear avoidance: Requirements and proposed system for airborne lidar detection. In *Airborne and Spaceborne Lasers for Terrestrial Geophysical Sensing, SPIE vol. 889*, pp. 54–64.